

Article

Study on the Adsorption, Diffusion and Permeation Selectivity of Shale Gas in Organics

Zhouhua Wang¹, Yun Li^{1,*}, Huang Liu¹, Fanhua Zeng², Ping Guo¹ and Wei Jiang³

¹ State Key Laboratory of Oil and Gas Reservoir Geology and Exploitation, Southwest Petroleum University, Chengdu 610500, China; wangzhouhua@126.com (Z.W.); liuhuangswwpu@sina.com (H.L.); guopingswpi@vip.sina.com (P.G.)

² Petroleum Systems Engineering, Faculty of Engineering and Applied Science, University of Regina, Regina, SK S4S 0A2, Canada; fanhua.zeng@uregina.ca

³ School of Chemical Engineering, Sichuan University, Chengdu 610065, China; weijiang@scu.edu.cn

* Correspondence: liyun930812@163.com; Tel.: +86-28-8303-5199

Academic Editor: Alireza Bahadori

Received: 26 October 2016; Accepted: 16 January 2017; Published: 23 January 2017

Abstract: As kerogen is the main organic component in shale, the adsorption capacity, diffusion and permeability of the gas in kerogen plays an important role in shale gas production. Based on the molecular model of type II kerogen, an organic nanoporous structure was established. The Grand Canonical Monte Carlo (GCMC) and Molecular Dynamics (MD) methods were used to study the adsorption and diffusion capacity of mixed gas systems with different mole ratios of CO₂ and CH₄ in the foregoing nanoporous structure, and gas adsorption, isosteric heats of adsorption and self-diffusion coefficient were obtained. The selective permeation of gas components in the organic pores was further studied. The results show that CO₂ and CH₄ present physical adsorption in the organic nanopores. The adsorption capacity of CO₂ is larger than that of CH₄ in organic pores, but the self-diffusion coefficient of CH₄ in mixed gas is larger than that of CO₂. Moreover, the self-diffusion coefficient in the horizontal direction is larger than that in the vertical direction. The mixed gas pressure and mole ratio have limited effects on the isosteric heat and the self-diffusion of CH₄ and CO₂ adsorption. Regarding the analysis of mixed gas selective permeation, it is concluded that the adsorption selectivity of CO₂ is larger than that of CH₄ in the organic nanopores. The larger the CO₂/CH₄ mole ratio, the greater the adsorption and permeation selectivity of mixed gas in shale. The permeation process is mainly controlled by adsorption rather than diffusion. These results are expected to reveal the adsorption and diffusion mechanism of gas in shale organics, which has a great significance for further research.

Keywords: adsorption diffusion; kerogen; molecular simulation; permeation selectivity; shale gas

1. Introduction

Recently, with the development and utilization of unconventional natural gas resources around the world, shale gas, as a kind of the unconventional gas, plays an important role in the exploration and development of natural gas reservoirs [1–3]. Among the various kinds of methods developed, hydraulic fracture technology is commonly applied in these reservoirs. Nevertheless, in order to reduce greenhouse gases around the world, CO₂ capture and sequestration technologies [4–6], tight gas and coalbed methane reservoir recovery by CO₂ injection and the method of exploring gas hydrates by CO₂ displacement have emerged [7–11]. Gas injection is considered an effective way to enhance oil and gas recovery and it has been widely used worldwide [12,13]. According to the adsorption capacity difference between CO₂ and CH₄ on shale [14–16], using CO₂ displacement to enhance the shale gas recovery has become one of the most promoted ways [17–19]. As the insoluble organics in shale,

kerogen is mainly composed of C, H and O and small amounts of the elements N and S, and it is an important material for gas production [20]. Most organics in shale are embedded in the inorganic mineral of the shale reservoir, and the organic pore size is about 5–250 nm [21]. The occurrence of fluids in the shale gas reservoir with organic nanopores is different from that seen in conventional gas reservoirs. Because of the large specific surface of shale, the content of gas adsorbed on the surface of clay mineral and organics should not be ignored. The content of adsorbed gas is about 5%–80% of the shale gas [22]. The diffusion of free gas in natural fractures is also important in the process of shale gas migration. Consequently, it is crucial to study the adsorption and diffusion of natural gas in organics, which provides a prominent understanding of the production and development of shale gas in the tight reservoirs.

Researchers have studied the mechanical properties of shale rock and the migration of shale gas through experimental and theoretical methods [23]. Chen proposed a new multilevel micromechanical homogenization scheme to predict the transversely isotropic properties of shale rock with the multi-inclusion and interfacial transition zone effects. By comparing the available experimental data with the theoretical data, the results of their research play an important role in determining the macroscopic properties of shale rocks [24]. By first discussing how shale is classified in relation to coal mining, Murphy researched the failure mechanics and intervention measures of shale in underground coal mines and shared the collective ground control experience of controlling roof structures dominated by shale rock in coal mining [25]. Nezhad proposed a simplified multiscale damage model to predict transversely isotropic shale rocks under tensile loading [26]. Nøtinger proposed the discrete fracture networks flow model to solve diffusion problems in complex three-dimensional (3D) fracture networks and researched the flow behavior of fluid in the matrix and fractures. Nøtinger pointed out that this method could be used to study the migration of oil and gas in unconventional shale [27]. Considering the effects of matrix-matrix and matrix-fracture molecular diffusion, Tao proposed a dual-permeability model to overcome the drawback of a single-porosity model. The simulation results demonstrated that matrix-matrix molecular diffusion and matrix-fracture molecular diffusion cannot be ignored in the process of gas injection except other factors [28].

With the development of modern experimental technology, the first step is to separate the organic matter from the shale. Most studies are based on organic solvent extraction. The disadvantage of this method is that the relevant information about the organics in clay mineral layers is easily ignored. The organics in the mixed layer minerals were extracted by using supercritical fluid and 12-aminolauric acid, respectively, and very good experimental results were obtained. It has been proved that the proportion of interlayer organics in the sample can be up to 50% of the total extraction [29,30]. The carbon skeleton structure of kerogen was obtained using a solid-state nuclear magnetic resonance (NMR) spectrum experiment [31]. The chemical group components, relative abundance and bond properties of kerogen were obtained by analyzing the position and intensity of infrared absorption bands in a thermogravimetry-infrared spectroscopy (TG-FTIR) coupled analysis. The structure and the electron images of kerogen were obtained by X-ray diffraction (XRD) and scanning electron microscopy (SEM), respectively, and then they were combined with the X-ray energy dispersive analysis to analyze the surface elements of kerogen. Based on the abovementioned experiments, the component, structure and structural parameters were obtained [32–34]. However, because kerogen is a complex polymer, using a variety of experimental analysis techniques to test the structure of kerogen requires considerable time and effort. On the one hand, the molecular structure of biological compounds is included in the test results. On the other hand, due to the complexity of the structural model, the structure characteristics of kerogen cannot be described accurately and systematically.

The rapid development of molecular simulation technology provides a convenient method for these studies. Researchers can now provide a reasonable prediction of molecular structure and the physical and chemical properties of kerogen. Simultaneously, the method has made certain progress in the research of shale and coal gas reservoirs. Hartman et al. used the Monte Carlo (MC) and

MD method to choose carbon nanotubes in place of the shale organics. The adsorption law of the mixtures was predicted by the IAS adsorption model, and a new equation was proposed to describe the adsorption phase densities of the mixtures [35,36]. Billemont et al. studied the adsorption law of CO₂, CH₄ and their mixtures by combining the experimental and molecular simulation methods and taking into account the adsorption law of gas under water preload conditions [37]. The results showed that the conclusion regarding gas adsorption was similar to that of previous research. However, in terms of the difference between experimental and simulation results, the authors proposed that the phase equilibrium between gas and water under different conditions should be considered [38,39]. Botan et al. used microporous carbon materials to replace the organic structure of shale and coal and simulated the separation process and the permeability of natural gas. The researchers found that this microporous material has no significant pressure gradient. Also, they found that the variation of permeability with temperature and pressure is consistent with diffusion theory. In the research process, carbon nanotubes and the disordered structure of carbon materials were used to replace the kerogen structure in shale [40]. By simulating the adsorption and diffusion characteristics of fluid in nanostructures, it is inevitable that there are some deficiencies. With domestic and foreign scholars' deep examination of this problem, the adsorption and diffusion process of shale gas and coalbed methane were studied using the average unit structure of organics or organic structure fragments. This has achieved good results for the adsorption and diffusion process of coalbed methane [41,42]. Hu et al. used a molecular simulation to research the adsorption and diffusion of CH₄ and CO₂ in coal. The results showed that the order of magnitude of CO₂ diffusion coefficient in coal was at 10⁻⁹ m²/s, which was close to the experimental results. Combined with the Maxwell-Stefan diffusion theory, Hu calculated the mutual diffusion coefficients of mixtures [43]. The adsorption capacity of CO₂ is greater than that of CH₄ under a certain temperature and pressure. Therefore, according to the law of competition adsorption between CO₂ and CH₄, Hu analyzed the basic principle of enhancing the gas recovery by CO₂ injection in a coal seam [44]. Liu et al. used the Density Functional Theory (DFT) and the GCMC method to research the adsorption of CO₂, H₂O, N₂ and the mixture of these gases on the coal, analyzing the adsorption capacity of fluid and considering the effect of moisture on it [45]. Based on the molecular model of wise coal and using the molecular simulation method to build the diffusion model of the CO₂/CH₄ mixture in coal pores. Zhao et al. analyzed the self-diffusion coefficient and transport diffusion coefficient under different conditions and studied the effect of temperature and gas mole fraction on diffusion coefficients. The results showed that the transport diffusion coefficient is larger than the corrected diffusion coefficient, and the corrected diffusion coefficient is larger than the self-diffusion coefficient. The three diffusion coefficients increased with temperature and the gas phase mole fraction increased gradually [46]. Meanwhile, scholars have researched the adsorption and diffusion of shale gas using molecular simulation methods. According to the ratio of C/H and C/O, Collell et al. established the structure of kerogen molecular fragments, used this structure to build the nanopore structure, and then used the GCMC and MD methods to study the adsorption characteristics of methane and ethane in this structure. At the same time, using the Extended Langmuir model and Ideal Adsorbed Solution (IAS) model to fit the experimental results, Collell found that the predicted results of the two models were consistent with the simulation results under low pressure conditions, but at high pressure, only a small part of the predicted results was in agreement with the simulation results, and the smaller the pores, the worse the match between the properties became [47]. In the same year, based on the experimental data, Collell used the molecular simulation method to obtain the molecular structure and the physical properties of shale organics and obtained the stable kerogen molecular structure by molecular dynamics simulation [48]. Based on the C/H and C/O ration of I, II and III kerogen, Ungerer et al. applied a molecular simulation method to establish a molecular structure model. The thermodynamic properties of different types of organics such as maturity, density, compressibility, swelling and adsorption isotherm were studied [20]. Hu [49] studied the change of gas and water distribution in organic pore by molecular dynamics simulation. The results showed that, if the kerogen pore is water wetted, the water molecules are adsorbed near

the functional groups and the methane molecules were adsorbed on the surface of the organics. Also, a gas-water two-phase exists within the pore. If the kerogen pore was non-wet, the methane molecules were adsorbed on the pore surface and the pores were filled with free gas. Falk et al. [50] utilized CS1000 and CS1000a as organic structures by using the Configuration-Bias Monte Carlo (CBMC) and MD to simulate the adsorption characteristics of long-chain paraffins on it at the actual temperature of the reservoir and it's the adsorption characteristic curve satisfied with the Langmuir isothermal adsorption model. Guan, et al. [51] analyzed the molecular structure information of Huadian oil shale and established the kerogen molecular structure by using NMR, X-ray photoelectron spectroscopy, Fourier transform infrared and a X ray diffraction experiment testing technique combined with DFT. Sui et al. [52] established the 3D structure of kerogen II and analyzed the pore size distribution (PSD) of this structure. Using the GCMC and MD methods, they studied the adsorption and diffusion of CO₂ and CH₄ gas molecules on the kerogen and the adsorption capacity, self-diffusion coefficient and radial distribution function (RDF) of CO₂ and CH₄. Falk et al. used molecular simulation and statistical mechanics to show the transmission behavior of hydrocarbon in shale nanoporous matrix, the results demonstrated that the Darcy's law fails to predict the transport of shale gas at the nanoscale. In particular, when studying on the transmission mechanism of shale gas in disordered pores, the influence of permeability, porosity and tortuosity should be considered [53]. It was found that whether the gas is adsorbed on coal or shale, the organics structure is the main research object.

On the basis of the literature review, we have investigated the adsorption and diffusion law of the gas in the organics, respectively, and different factors on adsorption and diffusion of gas are studied. We established the organic nanoporous structures based on type II kerogen. By simulating the adsorption and diffusion and analyzing the permeation selectivity of CO₂/CH₄ mixtures in the organics, this research has important significance for the further determination of mixed gas permeability in organic pores.

2. Simulation Details

2.1. Grand Canonical Monte Carlo (GCMC)

The Grand Canonical Monte Carlo (GCMC) is a simulation method which is calculated under selected ensemble conditions. It is a universal and effective method for research on adsorption and gas mixtures, and it has been widely used in the fields of engineering, economics and physics. In the field of geology, many scientists have used this method to evaluate oil and gas resources. The GCMC is a stochastic simulation method based on the probabilistic statistical theory. It uses computer simulation to establish a probabilistic model or stochastic process and obtain final results. At the same time, in order to improve the computational efficiency, the Metropolis sampling method is adopted in this study to simulate the random configuration of the microparticles.

In this paper, GCMC was used to study the adsorption behavior of gas in organics. According to the variation range of the temperature and pressure of a shale reservoir, the simulated temperature is 333.15 K, which is close to the formation temperature. The pressure range is 0–40 MPa. The three dimensional periodic boundary condition is used in the simulation process. The van der Waals is an atom-based method, and the electrostatic long-range effect is calculated using the Ewald summation method [54]. The simulation step number is 1×10^7 , and the total number is 3×10^7 . It outputs a structure every 6000 steps, which confirms that each adsorption simulation will reach a balanced state. The first half of process is used to guarantee adsorption equilibrium, and the latter half is used for ensemble average and for calculate the required parameters, such as adsorption isotherms and adsorption isosteric heat.

2.2. Molecular Dynamics (MD)

Molecular Dynamics (MD) is an integrated science and technology method based on molecular particles, atomic particles and other microscopic particles as the research object combined with the

physical, chemical and mathematical theories. Newton's equation is used to calculate the position, velocity and energy of particles at different times. The appropriate statistical method is used to obtain the physical parameters [55].

Based on the results of adsorption simulated, the MD method was used to simulate the diffusion of CH₄/CO₂ in kerogen. The trajectory of microparticles is calculated, and the diffusion mechanism is revealed from the micro level. At the beginning of the simulation, in order to ensure the simulation structure is optimal, the first step was to simulate the structure by using crystal lattice relaxation. Then, the canonical ensemble (NVT) MD was carried out to reach the equilibrium state. The time step was 1 femtosecond for all simulations. The total simulation time was 300 picosecond to ensure that the mean squared displacement is truly linear in time. The Hoover-Nosé method was used throughout the process to obtain the self-diffusion coefficients, radial distribution functions, etc.

2.3. Kerogen Molecule Structure

In research on bituminous structures, by using molecular simulation methods, the previously mentioned concept of "average molecular structure" refers to an atom aggregate that averages the number of aromatic clusters in the structure. It cannot be used as a special molecular structure or as the basic unit of the molecule [47]. In fact, the actual structure of kerogen does not exist as a single chemical structure. It is necessary to research all kinds of representative fragments and functional groups in order to establish the average molecular structure of kerogen. Considering the interaction between the atoms, functional groups, molecular structure and geometric morphology of kerogen, the molecular structure of the final kerogen was obtained. In this paper, we chose the representative kerogen of type II is chosen as the research object (in the following sections, it is just called kerogen) [18]. The chemical formula is C₂₅₂H₂₉₄O₂₄N₆S₃ and the molecular structure is shown in Figure 1.

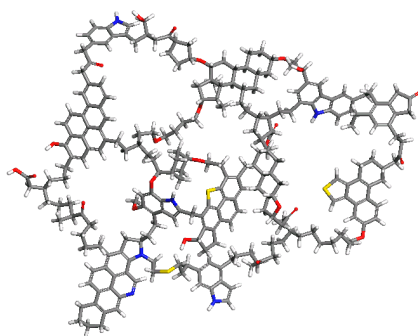


Figure 1. The molecular structure of kerogen.

3. Established the Structure of Organic Pore

According to the selected molecular structure of kerogen, the Amorphous Cell module of Accelrys Studio Material software is used to add periodic boundary conditions and a 3D periodic structure that contains six kerogen molecules is established. In order to obtain the stable periodic boundary model, the 3D kerogen molecular structure with periodic boundary must be optimized. Based on the initial structure model, the Geometry Optimization module was used to optimize this structure. The periodic boundary of the space lattice is gradually reduced until the stable configuration is obtained. The total energy of the model changes gradually during molecular mechanics and molecular dynamics optimization. In the process of optimizing kerogen structure by molecular dynamics, the total energy of the model is decreased first and then increased. Meanwhile, the structure corresponding to the minimum total energy is considered the most stable configuration. The simulated force field is COMPASS force field, which is widely applied to organics [56,57]. Finally, the isobaric-isothermal ensemble (NPT) of molecular dynamics is used to achieve the crystal lattice relaxation for the optimized model and obtain the stable 3D structure as shown in Figure 2a. The pore

size distribution of kerogen structure is shown in Figure 2b, while Figure 3 shows the size of the 3D structure: $3.305 \text{ nm} \times 3.305 \text{ nm} \times 3.305 \text{ nm}$. Density change is shown in Figure 4. It can be seen that the final density is 1.073 g/cm^3 . Because the actual density of kerogen is very difficult to test, there is a variation range between 0.8 and 2.2 g/cm^3 [58], the simulated result is within this range. The uncertainty concerning kerogen density arises mainly from the following aspects. On the one hand, although the experimental test ruled out the effect of clay minerals and other inorganic substances, the microelements existing in the form of non-minerals lead to the experimental test density being greater than the calculated density [59]. On the other hand, a great number of small molecules of substances exist in the actual kerogen structure, and it will fill in the kerogen pores.

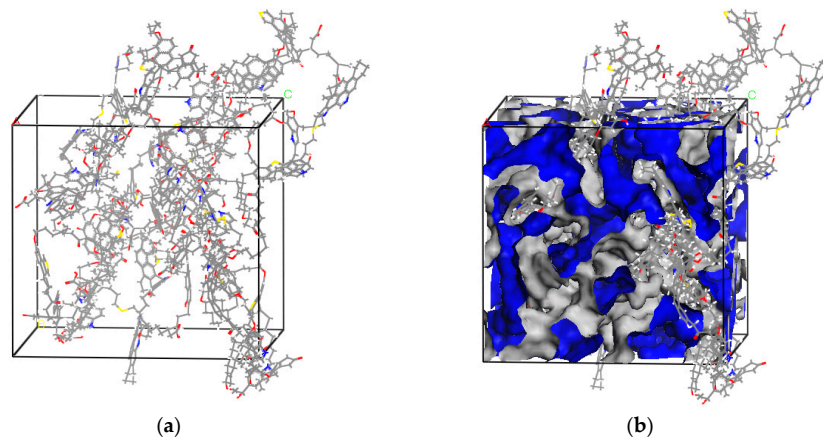


Figure 2. Kerogen model: (a) 3D model and (b) pore size distribution.

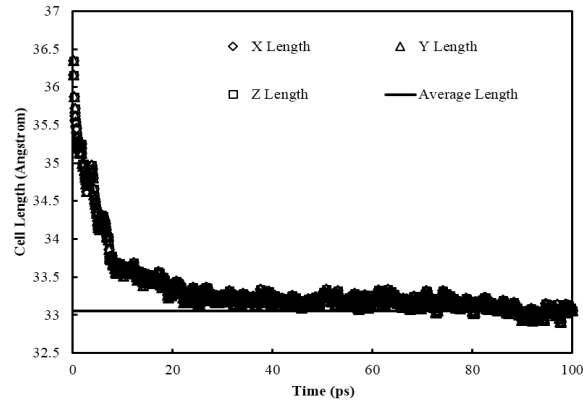


Figure 3. Simulated 3D size of kerogen.

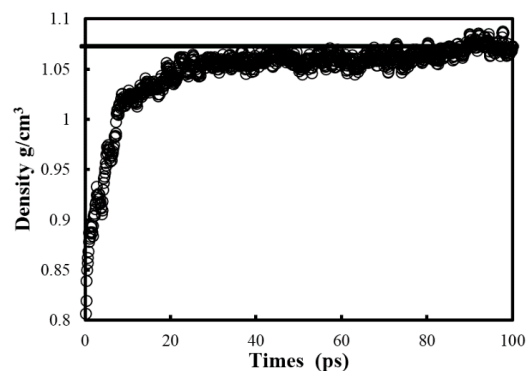


Figure 4. Simulated density of kerogen.

4. Results and Discussion

4.1. Adsorption Isotherms

Shale contains abundant organics. The adsorption capacity of CO_2 is stronger than that of CH_4 in organics. Therefore, it is theoretically feasible to enhance the recovery of shale gas by CO_2 injection [60]. In order to investigate the adsorption characteristics of CH_4/CO_2 mixture in organics pores, and the effect of CO_2 injection volume on the enhancement of CH_4 recovery, four different mole ratios of CH_4/CO_2 mixture gas were selected: 1:1, 1:2, 1:3 and 1:4. The adsorption isotherms of CH_4 and CO_2 under different pressure are then obtained, as shown in Figure 5.

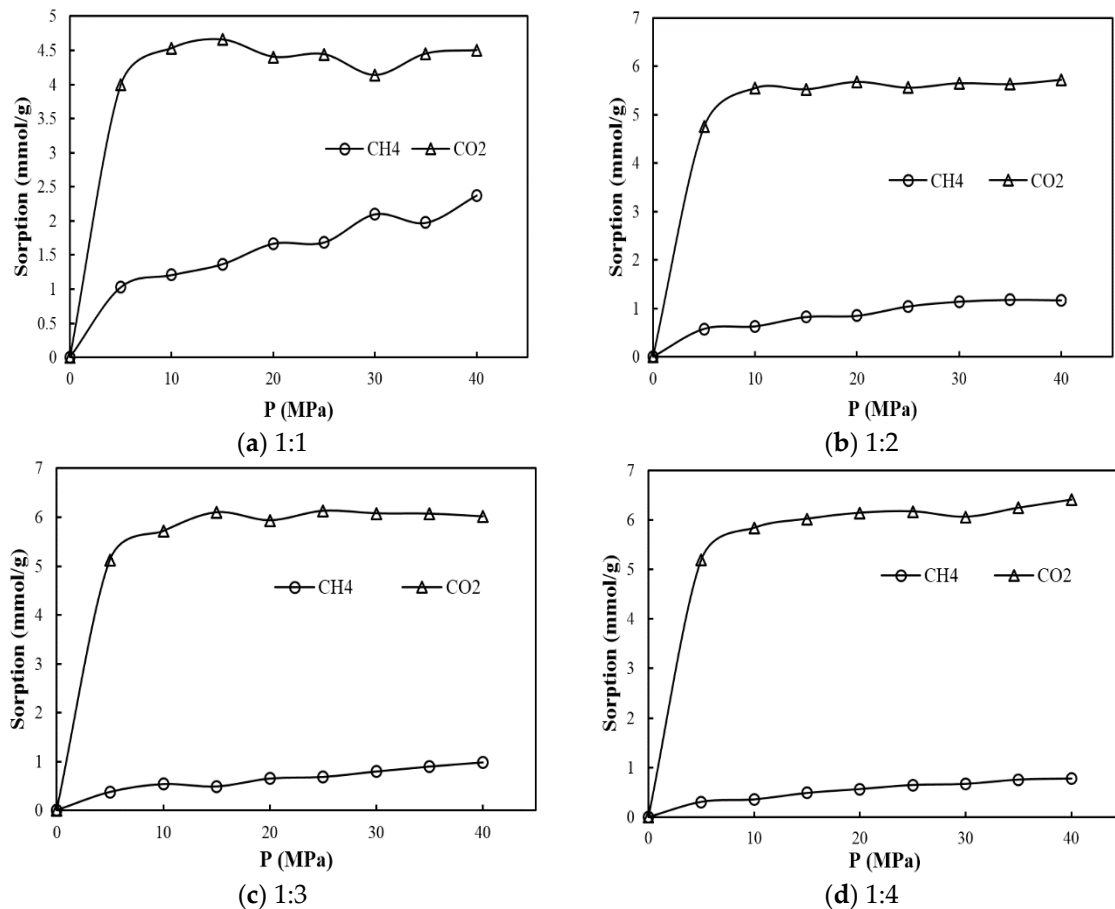


Figure 5. Adsorption isotherms of CH_4/CO_2 .

As can be seen from Figure 5, the adsorption capacity of CO_2 is much larger than that of CH_4 in kerogen. Meanwhile, the adsorption capacity of these gasses is increased by the increase of pressure. In the range of 0–20 MPa, the gas adsorption capacity increased with the increase of pressure. When the pressure reached 20 MPa, the adsorption process reached saturation adsorption. Also, the effect of pressure on the adsorption was very small. Under different molar ratio conditions, with the increase of the CO_2 concentration, the difference between the adsorption amount of CO_2 and CH_4 increased gradually because the partial pressure of CO_2 in the mixture increased under the same pressure. Therefore, in the process of increasing the yield of shale gas reservoir by injection CO_2 , by properly increasing the total ratio of injected gas CO_2 and the total CH_4 of shale gas reservoirs, a higher CH_4 recovery can be obtained. However, the results indicated that, with the increase of the mole ratio of CO_2 , the replacement efficiency of CH_4 remains constant at $\text{CH}_4:\text{CO}_2 < 4:1$. This may be due to CO_2

coverage on the surface of the kerogen under the corresponding conditions. Table 1 shows the change in the isosteric heat of adsorption with the pressure of the mixture in different proportions.

Table 1. The isosteric heat of adsorption of mixture in different proportions (Unit: KJ/mol).

Pressure (MPa)	1:1		1:2		1:3		1:4	
	CH ₄	CO ₂						
5	18.54	26.48	18.85	26.55	18.71	26.76	19.07	26.67
10	18.98	26.76	19.49	27.57	19.62	27.41	19.34	27.35
15	19.05	27.21	19.65	27.32	19.58	27.66	19.93	27.50
20	19.32	27.06	19.40	27.76	19.70	27.73	19.86	27.55
25	19.11	26.89	19.57	27.55	19.65	27.93	19.61	27.76
30	19.48	26.71	19.66	27.53	19.78	27.94	19.60	27.36
35	19.26	27.12	19.73	27.65	19.67	28.00	20.29	28.02
40	19.51	26.80	19.73	27.54	19.79	27.81	19.94	27.89

It can be seen that the isosteric heat of adsorption decreased first then increased with the increment of pressure. This result shows that at the start of adsorption, due to the surface heterogeneity of the kerogen pores, gas molecules prefer to adsorb in the higher energy positions. With the process of adsorption, the gas began to occupy the higher adsorption energy position and the isosteric heat of adsorption decreased gradually. As more gas molecules were adsorbed, the interaction between the molecules became stronger and their isosteric heat of adsorption became larger. This shows that the contribution of gas molecules to the heat of adsorption cannot be ignored as the adsorption progresses. The isosteric heat of adsorption of CO₂ is larger than that of CH₄, but they are less than 40 KJ/mol, and the adsorption heat of the chemical adsorption process is 40–600 kJ/mol [61]. Therefore, the adsorption of CH₄ and CO₂ on shale corresponds to physical adsorption.

4.2. Self-Diffusion

The diffusion law of gas in micronanometer pores is usually described by self-diffusion coefficient. The self-diffusion coefficient of shale gas in organics is calculated by Einstein equation [62]. Considering the interaction between CH₄ molecules, CH₄ and kerogen, in this paper, Equation (1) is used to calculate the Mean Square Displacement (MSD) of gas diffusion:

$$MSD = \left\langle \left| \vec{r}(t) - \vec{r}(0) \right|^2 \right\rangle = \left\langle \Delta r(t)^2 \right\rangle = \frac{1}{N} \sum_{i=1}^N \Delta r_i(t)^2 \quad (1)$$

According to the Einstein Equation, when describing the relationship between the MSD and time, the relationship between the slope and self-diffusion coefficient is as follows:

$$D_{self} = \lim_{t \rightarrow \infty} \frac{1}{6Nt} \left\langle \sum_{i=1}^N \left| \vec{r}_i(t) - \vec{r}_i(0) \right|^2 \right\rangle \quad (2)$$

Mean Square Displacement is usually fitted in a straight line, and the self-diffusion coefficient can be obtained from the 1/6 linear slope.

Due to the anisotropy of the kerogen molecular structure, in order to consider the influence of pore size and shape on the self-diffusion coefficient, the molecular dynamics simulation results were analyzed and the MSD data were output. The self-diffusion coefficients of gas in horizontal and vertical directions are calculated respectively [63], as shown in Figure 6.

Due to the anisotropy of the kerogen structure, the self-diffusion coefficients of gas in all directions are different. The self-diffusion coefficient in the horizontal direction (x, y direction) is significantly larger than that in the vertical direction (z direction). This result indicates that the resistance of gas in the horizontal direction is smaller, and it is the main direction for gas diffusion.

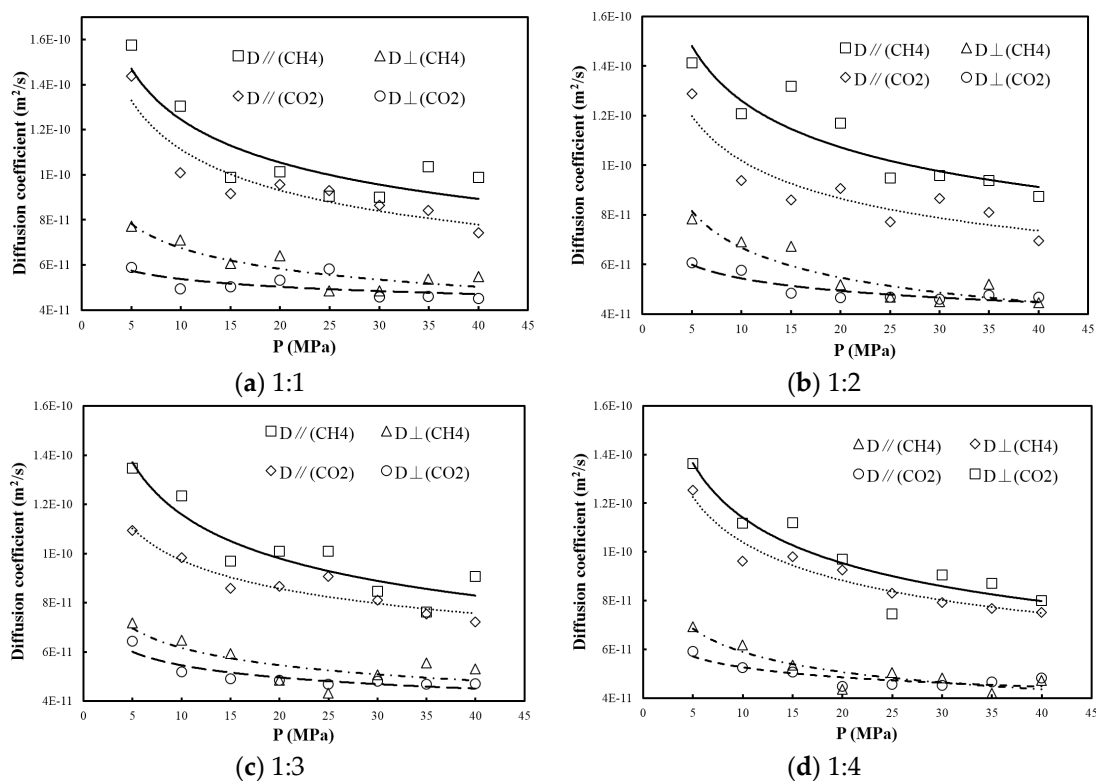


Figure 6. Self-diffusion coefficient of CH₄/CO₂ mixture in different directions.

It can be seen that the self-diffusion coefficient decreased with the increase of pressure in different directions. The self-diffusion coefficient in the horizontal direction obviously decreased. The self-diffusion coefficient of CH₄/CO₂ was gradually decreased with the increase of pressure. The molecules' self-diffusion coefficients tend to be consistent under higher pressure. This result shows that, with the increase of pressure, the density, the number of gas molecules and the probability of collisions between molecules were increased. The interaction between gas molecules became the key factor to control molecular diffusion. The self-diffusion coefficient of CO₂ is less than that of CH₄ under the same pressure. This is because the interaction between CO₂ molecules and kerogen is stronger than that of CH₄. Therefore, it will decrease the movement of a CO₂ molecule.

4.3. Radical Distribution Function (RDFS)

Next, we analyze the Radial Distribution Function (RDF) between the gas and the kerogen and learn more about their interactions in the simulation system. The RDF is defined as the ratio of the local density to average bulk density. This kind of research method describes the ordering degree of system structure, and it is usually used to characterize the microstructure of the particles [64]. The calculated expression is:

$$g(r) = \frac{dN}{4\pi\rho r^2 dr} \quad (3)$$

where $g(r)$ is RDF, N is the number of particles in the radius $r + dr$, and ρ is the density of particles.

From Figure 7, obvious main peaks were reached between CH₄, CO₂, N₂ and H₂O and atoms S, O and N in kerogen. Comparison of the peak values between CH₄, CO₂, N₂ and H₂O and atoms S, O and N shows that the interaction between CO₂ and atoms S and O in kerogen are much larger than that of CH₄ and N₂. This also implies that the adsorption capacity of CO₂ in the kerogen is larger than that of CH₄ and N₂. Two peaks appear in the RDF diagram between CO₂ and both atoms S and N.

This phenomenon indicates that the character of double-layer distribution near the S and N atoms, which causes the CO₂ adsorption capacity, outperforms that of CH₄ and N₂.

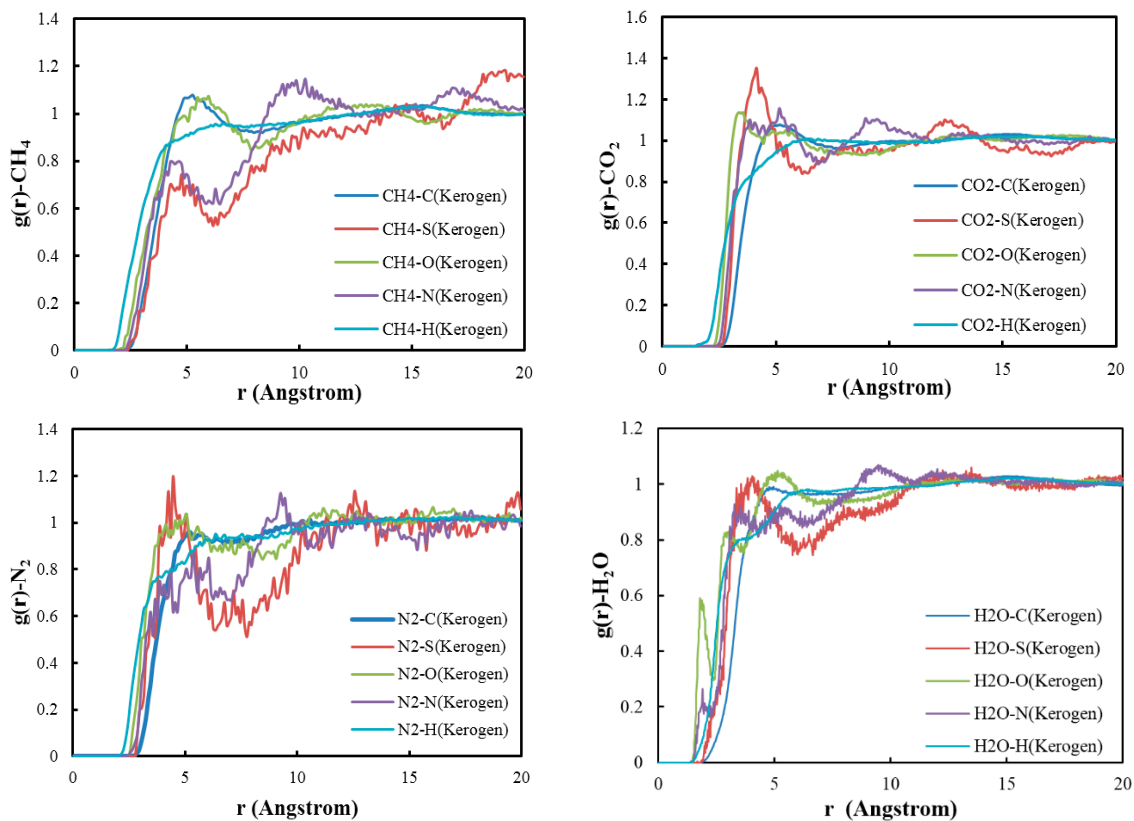


Figure 7. The RDF of CH₄, CO₂, N₂, H₂O and the atoms (C, H, O, N, S) in Kerogen.

4.4. Adsorption, Diffusion and Permeation Selectivity of Binary Gas

Finally, we investigated the permeation selectivity of CH₄/CO₂ in kerogen pores with different mole ratios. According to Equation (4), we first determined the adsorption selectivity and diffusion selectivity of mixed gas in kerogen. In the process of adsorption equilibrium, we used the adsorption selectivity (S_{sorp}) to determine the adsorption capacity of the gas mixture [65,66]:

$$S_{sorp} = \frac{x_{CO_2}/x_{CH_4}}{y_{CO_2}/y_{CH_4}} \quad (4)$$

where x_{CO_2} and x_{CH_4} represent the mole fraction of the gas component in the adsorbed phase, y_{CO_2} and y_{CH_4} and the bulk phase.

Diffusion selectivity refers to the ratio of mixture's fraction diffusion coefficient [67], the calculation formula is shown in Equation (5):

$$S_{diff} = \frac{D_{CO_2}}{D_{CH_4}} \quad (5)$$

Based on this Equation, the permeability coefficient of the CH₄/CO₂ can be obtained, as shown in Equation (6):

$$S_{perm} = \frac{x_{CO_2}/x_{CH_4}}{y_{CO_2}/y_{CH_4}} \cdot \frac{D_{CO_2}}{D_{CH_4}} \quad (6)$$

Figure 8 shows the adsorption selectivity, diffusion selectivity and permeation selectivity of CH₄/CO₂ with different molar ratios in kerogen.

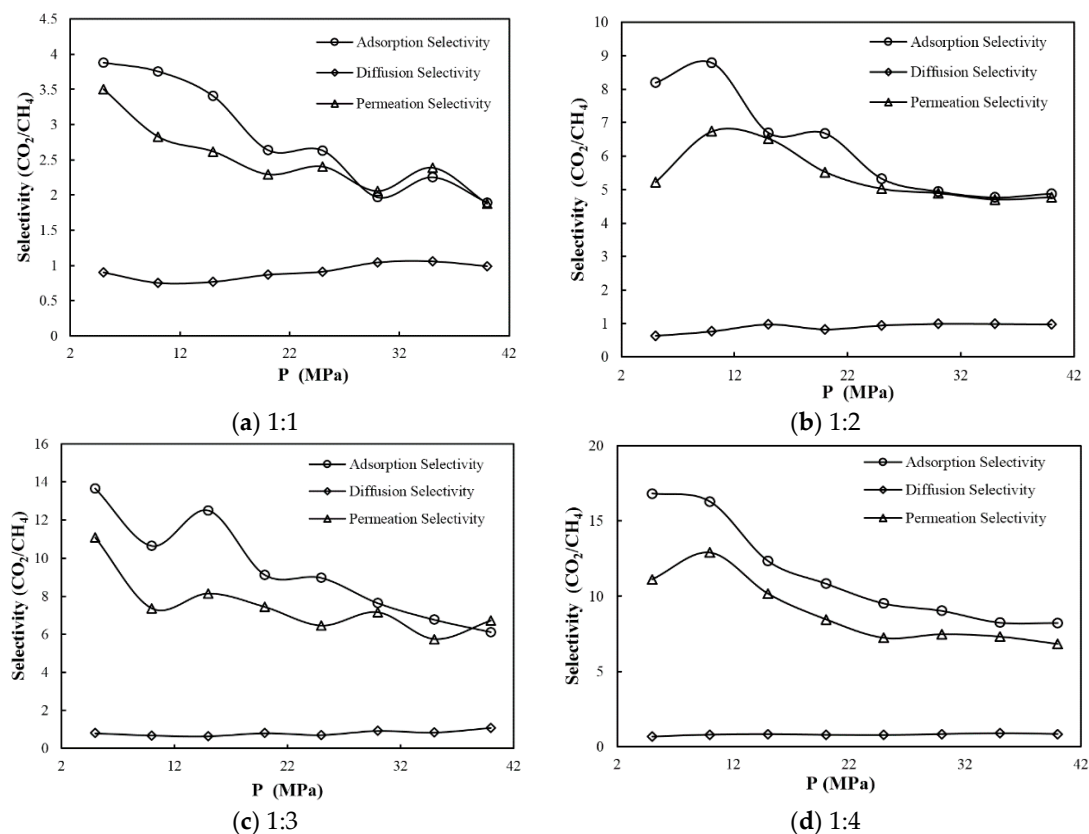


Figure 8. Adsorption, diffusion and permeation selectivity of CH₄/CO₂.

It can be seen that the adsorption selectivity coefficients of kerogen for CH₄/CO₂ mixed gas are always greater than 1. This indicates that the adsorption capacity of kerogen for CO₂ is greater than that of CH₄. With the increase of pressure, the adsorption selectivity gradually decreases and finally stabilizes. Meanwhile, with the increase of CO₂ in the mixed feed gas, the adsorption selectivity coefficient becomes correspondingly larger, but the diffusion selectivity coefficients are always less than 1, which explains that the diffusion capacity of CO₂ is less than that of CH₄ in kerogen, and the variation range of the diffusion coefficient is small in different proportions of CO₂ and CH₄ gas mixture. The mole ratio of CO₂ is higher in the mixed gas. The permeation selectivity coefficient of mixed gas is greater, which indicates the effect of CO₂ replacing CH₄ will be more obvious under the corresponding conditions.

5. Conclusions

According to the principles of GCMC and MD, we studied the interactions between kerogen and the different proportion of CH₄/CO₂ mixed gas and drew four conclusions:

- (1) In the range of 0–20 MPa, the adsorption capacity of the two gases (CH₄ and CO₂) increased with pressure. When the pressure reached 20 MPa, the adsorption capacity reached a certain saturation value, after which with the further increase of pressure, the amount of adsorption became very small. Pressure and the gas mole ratio had no significant effect on the isosteric heat of CH₄ and CO₂. The adsorption heat of CO₂ is higher than that of CH₄, and it was less than 42 KJ/mol, which lies in the physical adsorption range.
- (2) Due to the anisotropy of the kerogen structure, the self-diffusion coefficients of gas in all directions were different. The self-diffusion coefficient in the horizontal direction was significantly larger than that in vertical direction, and it decreased gradually with the increase of pressure. The self-diffusion coefficient of CO₂ is less than that of CH₄.

- (3) The interaction between CO₂ and S and O atoms in the kerogen was much larger than the interaction between CH₄ and N₂. Two peaks are evident for CO₂ and the S and N atoms in the radial distribution function diagram. This phenomenon indicates that the characteristic of double-layer distribution near the S and N atoms makes the CO₂ adsorption capacity outperform that of CH₄ and N₂.
- (4) The adsorption selectivity coefficients of the mixed gas of CO₂ and CH₄ in different proportions were normally greater than 1, while the diffusion selectivity was normally less than 1. This indicates that the adsorption capacity of CO₂ in kerogen was larger than that of CH₄, while its diffusion capacity was less than CH₄. The higher the molar ratio of CO₂ in the mixed gas, the adsorption selectivity of the mixed gas, and there was no obvious change in diffusion selectivity. This result shows that the mixed gas permeability is mainly influenced by the adsorption selectivity instead of by diffusion.

Acknowledgments: This research was supported by the National Natural Science Foundation of China (51204141, 51374179), National Scholarship Council Special Training Project Fund in the Western Region (201508515157).

Author Contributions: Zhouhua Wang and Yun Li conceived and designed the simulations; Zhouhua Wang, Yun Li, Huang Liu and Fanhua Zeng analyzed the data; Wei Jiang and Ping Guo contributed analysis tools; Zhouhua Wang and Yun Li wrote the paper.

Conflicts of Interest: The authors declare no conflict of interest.

References

1. Guo, C.; Xu, J.; Wu, K.; Wei, M.; Liu, S. Study on gas flow through nano pores of shale gas reservoirs. *Fuel* **2015**, *143*, 107–117. [[CrossRef](#)]
2. Wittcoff, H.A.; Reuben, B.G.; Plotkin, J.S. *Appendix D: The Importance of Shale Gas and Shale Oil*; John Wiley & Sons, Inc.: Hoboken, NJ, USA, 2013.
3. Wang, Q.; Chen, X.; Jha, A.N.; Rogers, H. Natural gas from shale formation—The evolution, evidences and challenges of shale gas revolution in United states. *Renew. Sustain. Energy Rev.* **2014**, *30*, 1–28. [[CrossRef](#)]
4. And, A.B.R.; Rubin, E.S. A technical, economic, and environmental assessment of amine-based CO₂ capture technology for power plant greenhouse gas control. *Environ. Sci. Technol.* **2002**, *36*, 4467–4475.
5. Macdowell, N.; Florin, N.; Buchard, A.; Hallett, J.; Galindo, A.; Jackson, G. An overview of CO₂ capture technologies. *Energy Environ. Sci.* **2010**, *3*, 1645–1669. [[CrossRef](#)]
6. Yang, M.; Song, Y.; Jiang, L.; Zhao, Y.; Ruan, X. Hydrate-based technology for CO₂ capture from fossil fuel power plants. *Appl. Energy* **2014**, *116*, 26–40. [[CrossRef](#)]
7. Zhou, L.; Feng, Q.; Chen, Z.; Liu, J. Modeling and upscaling of binary gas coal interactions in CO₂ enhanced coalbed methane recovery. *Procedia Environ. Sci.* **2012**, *12*, 926–939. [[CrossRef](#)]
8. Busch, A.; Gensterblum, Y. CBM and CO₂-ECBM related sorption processes in coal: A review. *Int. J. Coal Geol.* **2011**, *87*, 49–71. [[CrossRef](#)]
9. Zhao, J.; Xu, K.; Song, Y.; Liu, W.; Lam, W.; Liu, Y.; Xue, K.; Zhu, Y.; Yu, X.; Li, Q. A review on research on replacement of CH₄ in natural gas hydrates by use of CO₂. *Energies* **2012**, *5*, 399–419. [[CrossRef](#)]
10. Zhou, X.; Yu, Z. Phase Diagram Analysis and Dynamics Simulation on Replacement of Natural Gas Hydrate with CO₂. *Energy Dev. Front.* **2015**, *4*, 25–36.
11. Yuan, Q.; Sun, C.Y.; Liu, B.; Wang, X.; Ma, Z.W.; Ma, Q.L.; Yang, L.Y.; Chen, G.J.; Li, Q.P.; Li, S.; et al. Methane recovery from natural gas hydrate in porous sediment using pressurized liquid CO₂. *Energy Convers. Manag.* **2013**, *67*, 257–264. [[CrossRef](#)]
12. Wan, T.; Yu, Y.; Sheng, J.J. Experimental and numerical study of the EOR potential in liquid-rich shales by cyclic gas injection. *J. Unconv. Oil Gas Resour.* **2015**, *12*, 56–67. [[CrossRef](#)]
13. Gamadi, T.D.; Sheng, J.J.; Soliman, M.Y. An experimental study of cyclic CO₂ injection to improve shale oil recovery. In Proceedings of the SPE Improved Oil Recovery Symposium, Tulsa, OK, USA, 12–16 April 2014.
14. Ottiger, S.; Pini, R.; Storti, G.; Mazzotti, M. Competitive adsorption equilibria of CO₂ and CH₄ on a dry coal. *Adsorption* **2008**, *14*, 539–556. [[CrossRef](#)]
15. Duan, S.; Min, G.; Du, X.; Xian, X. Adsorption equilibrium of CO₂ and CH₄, and their mixture on Sichuan basin shale. *Energy Fuels* **2016**, *30*, 2248–2256. [[CrossRef](#)]

16. Wang, Z.; Li, Y.; Guo, P.; Meng, W. Analyzing the Adaption of Different Adsorption Models for Describing the Shale Gas Adsorption Law. *Chem. Eng. Technol.* **2016**, *39*, 1921–1932. [[CrossRef](#)]
17. Yuan, W.; Pan, Z.; Li, X.; Yang, Y.; Zhao, C.; Connell, L.D.; Li, S.; He, J. Experimental study and modelling of methane adsorption and diffusion in shale. *Fuel* **2014**, *117*, 509–519. [[CrossRef](#)]
18. Wang, B.; Byran, M.; Warren, G.; Sokol, P. Methane Adsorption and Diffusion in Nanoporous Gray Shale by QENS. In Proceedings of the American Physical Society March Meeting 2015, San Antonio, TX, USA, 2–6 March 2015.
19. Li, D.; Xu, C.; Wang, J.Y.; Lu, D. Effect of knudsen diffusion and langmuir adsorption on pressure transient response in tight-and shale-gas reservoirs. *J. Pet. Sci. Eng.* **2014**, *124*, 146–154. [[CrossRef](#)]
20. Ungerer, P.; Collett, J.; Yiannourakou, M. Molecular Modeling of the Volumetric and Thermodynamic Properties of Kerogen: Influence of Organic Type and Maturity. *Energy Fuels* **2015**, *29*, 91–105. [[CrossRef](#)]
21. Chan, Y.M.; Goh, K.L. Microscopic pore characteristics of sha-3 and sha-4 shale and their accumulation significance in liaohe depression. *Oil Gas Geol.* **2014**, *35*, 286–294.
22. Masters, J.A. Deep Basin Gas Trap in Western Canada. *AAPG Bull.* **1979**, *63*, 152–181.
23. Sone, H.; Zoback, M.D. Mechanical properties of shale-gas reservoir rocks—Part 1: Static and dynamic elastic properties and anisotropy. *Geophysics* **2013**, *78*, 381–392. [[CrossRef](#)]
24. Chen, Q.; Nezhad, M.M.; Fisher, Q.; Zhu, H.H. Multi-scale approach for modeling the transversely isotropic elastic properties of shale considering multi-inclusions and interfacial transition zone. *Int. J. Rock Mech. Min. Sci.* **2016**, *84*, 95–104. [[CrossRef](#)]
25. Murphy, M.M. Shale Failure Mechanics and Intervention Measures in Underground Coal Mines: Results from 50 Years of Ground Control Safety Research. *Rock Mech. Rock Eng.* **2016**, *2*, 1–11. [[CrossRef](#)] [[PubMed](#)]
26. Nezhad, M.M.; Zhu, H.; Ju, J.W.; Chen, Q. A simplified multiscale damage model for the transversely isotropic shale rocks under tensile loading. *Int. J. Damage Mech.* **2016**, *25*, 705–726. [[CrossRef](#)]
27. Nøttinger, B. A quasi steady state method for solving transient Darcy flow in complex 3D fractured networks accounting for matrix to fracture flow. *J. Comput. Phys.* **2015**, *1*, 205–223. [[CrossRef](#)]
28. Wan, T.; Sheng, J.J.; Li, L. Compositional Modeling of the Diffusion Effect on EOR Process in Fractured Shale Oil Reservoirs by Gas Flooding. *J. Can. Pet. Technol.* **2014**, *2*, 143–147.
29. Peng, Y.; Hongmei, L.; Dong, L. The catalysis of clay minerals in the process of oil and gas generation: A few thoughts. *Acta Mineral Sin.* **2012**, *32*, 70–71.
30. Lu, X.; Miao, D. Study of combination pattern of soluble organic matters and clay minerals in the immature source rocks in dongying depression, China. *Sci. Geol. Sin.* **1999**, *34*, 69–77.
31. Zhibin, W.; Xiuxiang, G.; Dajiang, Z.; Jiang, D. Assessment of thermal evolution of kerogen geopolymers with their structural parameters measured by solid-state ¹³C NMR spectroscopy. *Energy Fuels* **2005**, *19*, 240–250.
32. Wang, J.; Du, J.; Chang, L.; Xie, K. Study on the Structure and Pyrolysis Characteristics of Chinese Western Coals. *Fuel Process. Technol.* **2010**, *91*, 430–433. [[CrossRef](#)]
33. Zeng, Y.; Wu, C. Raman and Infrared Spectroscopic Study of Kerogen Treated at Elevated Temperatures and Pressures. *Fuel* **2007**, *86*, 1192–1200. [[CrossRef](#)]
34. Muhammad, A.F.; Salmawy, M.S.E.; Abdelaala, A.M.; Sameah, S. El-nakheil oil shale: Material characterization and effect of acid leaching. *Oil Shale* **2011**, *28*, 528–547. [[CrossRef](#)]
35. Hartman, R.C.; Ambrose, R.J.; Akkutlu, I.Y.; Clarkson, C.R. Shale Gas-in-Place Calculations Part II—Multicomponent Gas Adsorption Effects. *J. Soc. Pet. Eng.* **2011**. [[CrossRef](#)]
36. Bartuś, K.; Bródka, A. Methane in carbon nanotube: Molecular dynamics simulation. *Mol. Phys.* **2011**, *109*, 1691–1699. [[CrossRef](#)]
37. Billemont, P.; Coasne, B.; De, W.G. Adsorption of carbon dioxide, methane, and their mixtures in porous carbons: Effect of surface chemistry, water content, and pore disorder. *Langmuir* **2013**, *29*, 3328–3338. [[CrossRef](#)] [[PubMed](#)]
38. Zhou, Y.; Sun, W.; Chu, W.; Liu, X.; Jing, F.; Xue, Y. Theoretical insight into the enhanced CH₄ desorption via H₂O adsorption on different rank coal surfaces. *J. Energy Chem.* **2016**, *25*, 677–682. [[CrossRef](#)]
39. Li, J.; Li, X.; Wang, X.; Li, Y.; Wu, K.; Shi, J.; Yang, L.; Feng, D.; Zhang, T.; Yu, P. Water distribution characteristic and effect on methane adsorption capacity in shale clay. *Int. J. Coal Geol.* **2016**, *159*, 135–154. [[CrossRef](#)]
40. Boğan, A.; Vermorel, R.; Ulm, F.J.; Pellenq, R.J. Molecular simulations of supercritical fluid permeation through disordered microporous carbons. *Langmuir* **2013**, *29*, 9985–9990. [[CrossRef](#)] [[PubMed](#)]

41. And, F.H.; Lu, G.Q. Adsorption Characteristics of Phenolic Compounds onto Coal-Reject-Derived Adsorbents. *Energy Fuels* **1998**, *12*, 1100–1107.
42. Xiang, J.H.; Zeng, F.G.; Liang, H.Z.; Li, B.; Song, X.X. Molecular simulation of the CH₄/CO₂/H₂O adsorption onto the molecular structure of coal. *Sci. China Earth Sci.* **2014**, *57*, 1749–1759. [[CrossRef](#)]
43. Hu, H.; Li, X.; Fang, Z.; Wei, N.; Li, Q. Small-molecule gas sorption and diffusion in coal: Molecular simulation. *Energy* **2010**, *35*, 2939–2944. [[CrossRef](#)]
44. Hu, H.; Du, L.; Xing, Y.; Li, X. Detailed study on self- and multicomponent diffusion of CO₂-CH₄ gas mixture in coal by molecular simulation. *Fuel* **2017**, *187*, 220–228. [[CrossRef](#)]
45. Liu, X.Q.; He, X.; Qiu, N.X.; Yang, X.; Tian, Z.Y.; Li, M.J.; Xue, Y. Molecular simulation of CH₄, CO₂, H₂O and N₂ molecules adsorption on heterogeneous surface models of coal. *Appl. Surf. Sci.* **2016**, *389*, 894–905. [[CrossRef](#)]
46. Zhao, Y.; Feng, Y.; Zhang, X. Molecular simulation of CO₂/CH₄ self - and transport diffusion coefficients in coal. *Fuel* **2016**, *165*, 19–27. [[CrossRef](#)]
47. Collell, J.; Galliero, G.; Gouth, F.; Montel, F.; Pujol, M.; Ungerer, P.; Yiannourakou, M. Molecular simulation and modelisation of methane/ethane mixtures adsorption onto a microporous molecular model of kerogen under typical reservoir conditions. *Microporous Mesoporous Mater.* **2014**, *197*, 194–203. [[CrossRef](#)]
48. Collell, J.; Ungerer, P.; Galliero, G.; Yiannourakou, M.; Montel, F.; Pujol, M. Molecular simulation of bulk organic matter in type II shales in the middle of the oil formation window. *Energy Fuels* **2014**, *28*, 7457–7466. [[CrossRef](#)]
49. Hu, Y.; Devegowda, D.; Striolo, A.; Civan, F.; Sigal, R.F.; Hu, Y. Microscopic dynamics of water and hydrocarbon in shale-kerogen pores of potentially mixed-wettability. *SPE J.* **2013**, *20*, 112–124. [[CrossRef](#)]
50. Falk, K.; Pellenq, R.; Ulm, F.J.; Coasne, B. Effect of chain length and pore accessibility on alkane adsorption in kerogen. *Energy Fuels* **2015**, *29*, 7889–7896. [[CrossRef](#)]
51. Guan, X.H.; Liu, Y.; Wang, D.; Wang, Q.; Chi, M.S.; Liu, S.; Liu, C. Three-dimensional structure of a huadian oil shale kerogen model: An experimental and theoretical study. *Energy Fuels* **2015**, *29*, 4122–4136. [[CrossRef](#)]
52. Sui, H.; Yao, J. Effect of surface chemistry for CH₄/CO₂ adsorption in kerogen: A molecular simulation study. *J. Nat. Gas Sci. Eng.* **2016**, *31*, 738–746. [[CrossRef](#)]
53. Falk, K.; Coasne, B.; Pellenq, R.; Ulm, F.J.; Bocquet, L. Subcontinuum mass transport of condensed hydrocarbons in nanoporous media. *Nat. Commun.* **2014**, *6*, 6949. [[CrossRef](#)] [[PubMed](#)]
54. Li, W.; Fang, X.; Li, B.; Zeng, F. Molecular simulation of the sorption of methane and carbon dioxide in the montmorillonite. *J. Northeast Pet. Univ.* **2014**, *16*, 1021–1029.
55. Gui, L.Y.; Chen, L.J. Molecular simulation in chemical engineering. *Mod. Chem. Ind.* **2001**, *21*, 10–15.
56. Bunte, S.W.; Sun, H. Molecular modeling of energetic materials: The parameterization and validation of nitrate esters in the COMPASS force field. *J. Phys. Chem. B* **2000**, *104*, 2477–2489. [[CrossRef](#)]
57. Sun, H. COMPASS: An ab initio force-field optimized for condensed-phase applications overview with details on alkane and benzene compounds. *J. Phys. Chem. B* **1998**, *102*, 7338–7364. [[CrossRef](#)]
58. Bousige, C.; Ghimbeu, C.M.; Vixguterl, C.; Pomerantz, A.E.; Suleimenova, A.; Vaughan, G.; Garbarino, G.; Feygenson, M.; Wildgruber, C.; Ulm, F.J.; et al. Realistic molecular model of kerogen's nanostructure. *Nat. Mater.* **2016**, *15*, 576–582. [[CrossRef](#)] [[PubMed](#)]
59. Li, Z.; Ward, C.R.; Gurba, L.W. Occurrence of non-mineral inorganic elements in macerals of low-rank coals. *Int. J. Coal Geol.* **2010**, *81*, 242–250. [[CrossRef](#)]
60. Zhang, G.D.; Zhou, W.; Ji, S.C.; Liu, J.Y.; Zhang, J.; Yang, H.H. Experimental study on CO₂ replacement method used in shale gas exploration. *J. Chengdu Univ. Technol.* **2015**, *42*, 366–371.
61. Zhang, T.; Ellis, G.S.; Ruppel, S.C.; Milliken, K.; Yang, R. Effect of organic-matter type and thermal maturity on methane adsorption in shale-gas systems. *Org. Geochem.* **2012**, *47*, 120–131. [[CrossRef](#)]
62. Einstein, A. On the movement of small particles suspended in a stationary liquid demanded by the molecular-kinetic theory of heat. *Ann. Phys.* **1905**, *17*, 549–560. [[CrossRef](#)]
63. Botan, A.; Marry, V.; Rotenberg, B. Diffusion in bulk liquids: Finite-size effects in anisotropic systems. *Mol. Phys.* **2015**, *113*, 1–6. [[CrossRef](#)]
64. Park, S.H.; Sposito, G. Monte Carlo simulation of total radial distribution functions for interlayer water in Li-, Na-, and K-montmorillonite hydrates. *J. Phys. Chem. B* **2000**, *104*, 4642–4648. [[CrossRef](#)]

65. Lu, L.; Wang, S.; Müller, E.A.; Cao, W.; Zhu, Y.; Lu, X.; Jackson, G. Adsorption and separation of CO₂/CH₄ mixtures using nanoporous adsorbents by molecular simulation. *Fluid Phase Equilibria* **2014**, *362*, 227–234. [[CrossRef](#)]
66. Jia, Y.; Wang, M.; Gao, L.W.C. Separation of CO₂/N₂ Gas Mixture through Carbon Membranes: Monte Carlo Simulation. *Sep. Sci. Technol.* **2007**, *42*, 3681–3695. [[CrossRef](#)]
67. Keskin, S. Adsorption, Diffusion, and Separation of CH₄/H₂ Mixtures in Covalent Organic Frameworks: Molecular Simulations and Theoretical Predictions. *J. Phys. Chem. C* **2012**, *116*, 2487–2500. [[CrossRef](#)]



© 2017 by the authors; licensee MDPI, Basel, Switzerland. This article is an open access article distributed under the terms and conditions of the Creative Commons Attribution (CC BY) license (<http://creativecommons.org/licenses/by/4.0/>).